IX International Conference on Computational Methods in Marine Engineering
MARINE 2021
I.M. Viola and F. Brennan (Eds)

DEVELOPMENTS IN COUPLED HIGH-FIDELITY SIMULATIONS OF MOORED MARINE STRUCTURES

CLAES ESKILSSON[*,†] AND JOHANNES PALM[‡]

[*]Department of the Built Environment
Aalborg University
Thomas Manns Vej 23, DK-9220 Aalborg Ø, Denmark
e-mail: claese@build.aau.dk - Web page: http://build.aau.dk

[†] Renewable Energy Unit
Research Institutes of Sweden (RISE)
Box 857, SE-50115 Borås, Sweden
e-mail: claes.eskilsson@ri.se - Web page: http://www.ri.se

[‡] Sigma Energy & Marine AB
Ekelundsgatan 1-3, SE-41118 Gothenburg, Sweden
e-mail: johannes.palm@sigma.se - Web page: http://www.sigmaenergyandmarine.se

Key words: Mooring systems, Cable dynamics, Moody, Floating bodies, CFD, OpenFOAM

Abstract. Coupled mooring analysis using CFD with dynamic mooring models is becoming an established field. This is an important step for better predictions of responses of moored marine structures in extreme sea states and also for capturing the low-frequency response correctly. The coupling between the CFD and mooring solvers are most often carried out by exchanging the fairlead/anchor points and fairlead forces. In this paper we will discuss effects of using (i) viscous fluid flow on a mooring component level (submerged buoys and clump weights) and (ii) the fluid-structure coupling between the viscous fluid solver and the mooring system.

1 INTRODUCTION

Simulation of moored marine structures, including floating offshore renewable devices, are traditionally carried out using tools based on linear potential flow theories with dynamic mooring models. The two most common models for mooring dynamics are the lumped-mass approximation (such as the well-known OrcaFlex [1] software) and the linear finite element model, (such as in ANSYS-AQWA [2]). When the moored structure is simulated in CFD, the fidelity of the wave-structure interaction increases significantly, but the mooring models have traditionally been reduced to linear springs [3, 4] or quasi-static moorings. However, coupled mooring analysis using viscous Reynolds-Averaged Navier-Stokes equations (RANS) has started to become established [5, 6, 7, 8]. This is an important step for better predictions of responses in extreme sea states and also for capturing low-frequency response correctly [9]. In this paper we outline

and discuss recent developments in the mooring dynamics software Moody [10], and how it can be used for such analysis. Moody is based on an *hp*-adaptive discontinuous Galerkin method and comes with an API for coupling to different fluid solvers e.g., the two-phase RANS solver in OpenFOAM. In this paper we will look at the next steps in coupled mooring analysis using CFD such as:

- using viscous fluid flow directly on a mooring component level, e.g. for submerged buoys and clump weights used in hybrid mooring systems;
- the fluid-structure coupling between the viscous fluid solver and the mooring system. So far, this coupling has mostly been driven by exchange of the fairlead/anchor points and fairlead forces. The drag and inertia forces acting on the mooring line are typically given by linear potential flow computed inside the mooring solver. Here we will look into the effect of using a one-sided coupling (sampling of fluid in the RANS part to be used for drag and inertia in the mooring solver)

2 MOORING SOLVER

2.1 Equations for a elastic cable

A cable of length L is parametrised in the three inertial coordinates by a position vector $\vec{r}^{\,c} = \left[r_x^c(s), r_y^c(s), r_z^c(s)\right]^{\mathrm{T}}$, where $s \in [0, L]$ is the unstretched cable coordinate. The equation of motion for chains and ideally flexible lines (neglecting bending stiffness) becomes

$$\gamma_0 \frac{\partial^2 \vec{r}^{\,c}}{\partial t^2} = \frac{\partial}{\partial s}\left(\frac{T(\epsilon,\,\dot{\epsilon})}{1+\epsilon}\frac{\partial \vec{r}^{\,c}}{\partial s}\right) + \vec{f}^{\,c}\,, \tag{1}$$

$$\varepsilon = \left|\frac{\partial \vec{r}^{\,c}}{\partial s}\right| - 1\,, \tag{2}$$

where γ_0 is the cable mass per unit length, ϵ is the cable strain, and $\dot{\epsilon}$ is the strain-rate. The axial tension, $T(\epsilon,\,\dot{\epsilon})$, is a function of the strain and constitutes the cable material properties. As an example, a linear visco-elastic cable is described by $T = EA_0\epsilon + \xi\dot{\epsilon}$ in which EA_0 is the axial stiffness and ξ is the internal damping coefficient. The external forces are grouped in the variable $\vec{f}^{\,c}$, and contains the hydrodynamic forces of added mass, buoyancy and drag from the Morison equation [11] and contact forces from the ground $\vec{f}^{\,g}$. In this paper, we will primarily discuss the hydrodynamic fores, and no further details about the sea-floor contact model is presented. See [12] for more information on the ground model.

$$\vec{f}^{\,c} = \vec{f}^{\,a} + \vec{f}^{\,b} + \vec{f}^{\,d} + \vec{f}^{\,g}\,, \tag{3}$$

$$\vec{f}^{\,a} = \rho A_0\left(\vec{a}_{\mathrm{f}\perp} + C_{\mathrm{m}\imath}\vec{a}^{\,*}_{\imath} + C_{\mathrm{m}\perp}\vec{a}^{\,*}_{\perp}\right)\,, \tag{4}$$

$$\vec{f}^{\,b} = (A_0\rho - \gamma_0)g\hat{z}\,, \tag{5}$$

$$\vec{f}^{\,d} = 0.5d\rho\sqrt{1+\epsilon}\left(C_{\mathrm{d}\imath}\left|\vec{v}^{\,*}_{\imath}\right|\vec{v}^{\,*}_{\imath} + C_{\mathrm{d}\perp}\left|\vec{v}^{\,*}_{\perp}\right|\vec{v}^{\,*}_{\perp}\right)\,, \tag{6}$$

Here, index $\imath$ denotes the tangential projection of a vector onto the cable direction, and $\perp$ the remaining normal components. $\vec{v}^{\,*}$ and $\vec{a}^{\,*}$ denote the relative velocity and acceleration between the water and the cable respectively. The hydrodynamic coefficients C_{m} refer to added mass, and C_{d} refer to drag. Equations (1) and (2) are solved with the Moody mooring solver using an *hp*-adaptive discontinuous Galerkin method.

2.2 High-order discontinuous Galerkin method

The computational domain Ω is partitioned into N_{el} elements $\Omega_e \in [s_L^e, s_R^e]$ of element size h^e. A function $g(s,t)$ is approximated to an arbitrary order P within Ω^e as:

$$g(s,t) \approx g^e(s,t) = \sum_{k=0}^{k=P} \phi_k(s) \tilde{g}_k^e(t)\,, \tag{7}$$

where $\tilde{g}_k^e$ is the k:th order expansion coefficient to trial function $\phi_k(s)$. Legendre polynomials are used as test and trial functions to obtain a diagonal local mass matrix. Also, let us define

$$(a(s,t), b(s,t))_{\Omega^e} = \int_{\Omega^e} a(s,t) b(s,t) \mathrm{d}s\,, \tag{8}$$

as the inner product operator $(\quad)_{\Omega^e}$. Expressed in strong form within Ω^e, the DG formulation reads:

$$(\phi_l,\, \phi_m)_{\Omega^e}\, \tilde{\dot{u}}^e = \left(\phi_l,\, \frac{\partial \phi_m}{\partial \xi}\right)_{\Omega^e} \tilde{F}^e + \left[\widehat{\vec{F}} - \vec{F}^+\right]_{s_L^e}^{s_R^e} + (\phi_l,\, G)_{\Omega^e}\ . \tag{9}$$

A numerical flux (denoted with $\widehat{\cdot}$ in Equation (9)) is in the DG method used to express the boundary value of a quantity. Moody uses fluxes according to:

$$\widehat{\vec{F}} = \frac{1}{2}\left(\vec{F}^+ + \vec{F}^- + \lambda\left(n^- \vec{u}^+ + n^+ \vec{u}^-\right)\right)\,, \tag{10}$$

$$\lambda = \sqrt{\frac{1}{\gamma_0}\frac{\partial T}{\partial \epsilon}}\,, \tag{11}$$

where n is the outward pointing unit normal, λ is the speed of sound in the cable and $\widehat{\vec{F}}$ is the Lax–Friedrichs flux of $\vec{F}$. Superscripts $^+$ and $^-$ tell if values are taken from the interior domain (from Ω^e) or from the neighbouring element (Ω^{e+1} or Ω^{e-1} respectively). See [12] for details.

2.3 Coupled CFD solver for moored objects

The force and moment from the fluid acting on each computational face of the body surface is computed from the fluid pressure p_i and the shear stress τ_i of the surrounding flow. The rigid-body motion is governed by Newton's II law

$$\frac{\mathrm{d}}{\mathrm{d}t}\left(\mathbf{M}^f \vec{u}\right) = \sum_{i=1}^{N_{\text{cell}}} A_i \begin{bmatrix} p_i \hat{\mathrm{n}}_i + \vec{\tau}_i \\ r_i \times (p_i \hat{\mathrm{n}} + \vec{\tau}_i) \end{bmatrix} + \sum_{i=1}^{N} r_i \times \vec{F}_i\,, \tag{12}$$

where r_i is the position vector from the centre of gravity to the cell face-centre or the mooring attachment point respectively, $\hat{\mathrm{n}}_i$ is the unit outward-pointing normal of face i and A_i is the face area. The total number of cells on the body surface is N_{cell}. Here the fundamental coupling between the mooring and the CFD domains is evident. The sum of N mooring line forces $\vec{F}_i$ is added to the rigid-body motion equation.

The mooring force computed by Moody acts as a restraint to the rigid body solver in the CFD domain. For details and validation of the coupling see [6, 10]. The connection with Moody was made using the interpolation scheme of Moody API. The typical time step size for the mooring cables in these simulations is at least an order of magnitude smaller than the time step used in the fluid part. A quadratic interpolation of attachment point position was used to sub-step the position boundary condition of the mooring solver.

2.4 CFD to resolve mooring components

A less common application of coupled CFD–mooring simulations is to resolve mooring components (submerged buoys or clump weights) in CFD. The forces and moments acting on the mooring component follow directly as for any other body, see eq. (12). CFD clearly carries a heavy computational burden, but if the main floater is to be resolved in CFD the extra cost can be justified. Also, for larger submerged buoys relatively near the surface or even surface piercing, the flow may be complicated enough to justify the extra effort.

2.5 Fluid sampling

This type of simulation introduces another functionality to the CFD-mooring simulation palette. Mooring cables are thin structures that often have little impact on the surrounding water motion due to current or waves. As long as regions where there is a risk of large vortex-induced-motion (VIM) are avoided, a one-sided coupling is therefore a good approximation to increase the fidelity of the resulting mooring loads. In this one-sided coupling, the fluid motion in the CFD domain is allowed to influence the mooring simulation via the parameterised Morison approximation. But the effect of the cable motion in the flow is not simulated, hence a one-sided coupling. This simplification allows for the moorings to move also in regions of coarser mesh. The loads on the system are from [11], according to eqs. (4) - (6). The flow-chart in Figure 1 explains the working principle of the fluid velocity sampling.

At each time-step, the CFD solver collects important sampling points from the mooring solver. In the current implementation we use the quadrature points of the Legendre polynomials, however a coarser sampling may very well be justified. The mooring points are converted to fluid probes, which sample the fluid density (ρ), the velocity (U), and the acceleration $\left(\frac{\partial U}{\partial t}\right)$. The sampled fluid state data is used by Moody to determine the effective level of submergence for each line element, as well as flow-dependent Morison loads from added mass and drag effects. The domain sizes of the two solvers are allowed to be different, so for any point where the mooring lines are extending beyond the CFD domain, the fluid is assigned to be quiescent, and the density is selected based on the still water level.

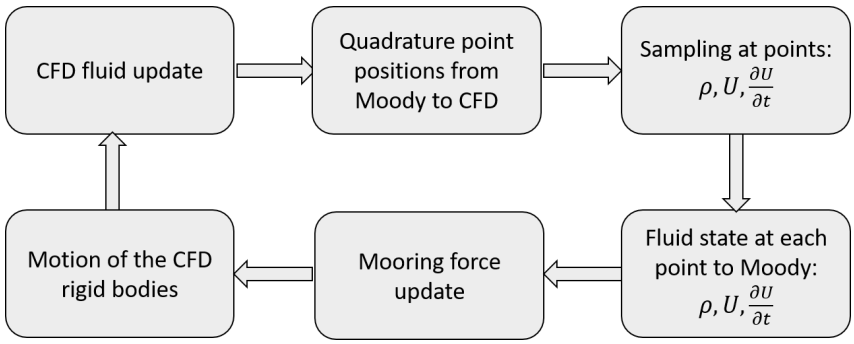

Figure 1: Flow-chart of one-sided sampling implementation.

3 TEST CASES

3.1 CFD modelling of a mooring component (submerged buoy)

Mooring component simulation can be done in several different ways. In this case, a mooring component is a submerged buoy or clump-weight, which is of substantial size. Palm and Eskilsson [13] have shown a detailed analysis of the response of three cylindrical submerged buoys using four different numerical methods. The cylinder shown here has $D = 2.1$ m diameter, 8.4 m^3 volume and a reserve buoyancy of 55 kN. It is attached -1.837 m below its center of volume to two mooring lines of polyester (80 mm nominal diameter). Figure 2 shows the layout of the mooring leg and the cfd-mesh of the cylinder at rest. The cylinder was simulated moving in still water with the entire computational domain. The four methods used were:

1. *xyz* - Only translation implemented in the buoy motion. Rotation is neglected, and ignored;
2. *ind* - The Morison drag loads due to rotating the buoy are computed independently from the loads originating from the translating motion;
3. *quad* - In the quad method, the coupling between translation and rotation of the buoy is solved using numerical quadrature along the symmetry axis;
4. *cfd* - As a final step in fidelity, a full RANS simulation is used for loads influencing the buoy motion.

Figure 3 shows the difference in result between different levels of fidelity used for estimating the buoy and mooring response. The *xyz* method is deviating considerably from the other three methods. From this we conclude that the rotational mode of motion has a large impact on the motion response of both the buoy and the mooring load. The *cfd* simulation matches relatively well with the *quad* and *ind* methods in terms of mooring force range, however, the

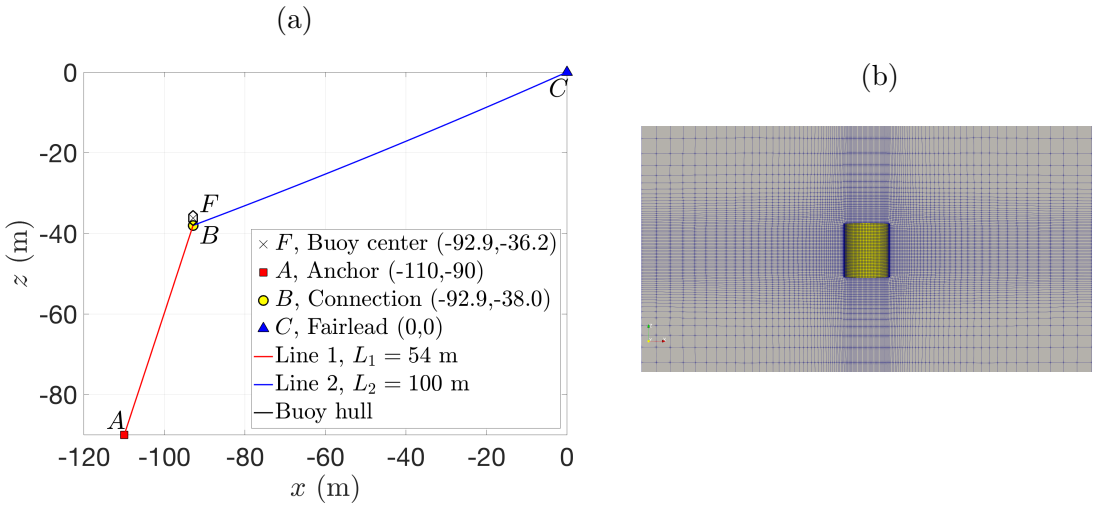

Figure 2: (a): Layout of the mooring system at equilibrium, showing the location of points *A, B, C* and *F* in the mooring leg. (b): Two-dimensional view of the buoy dimensions in the CFD domain.

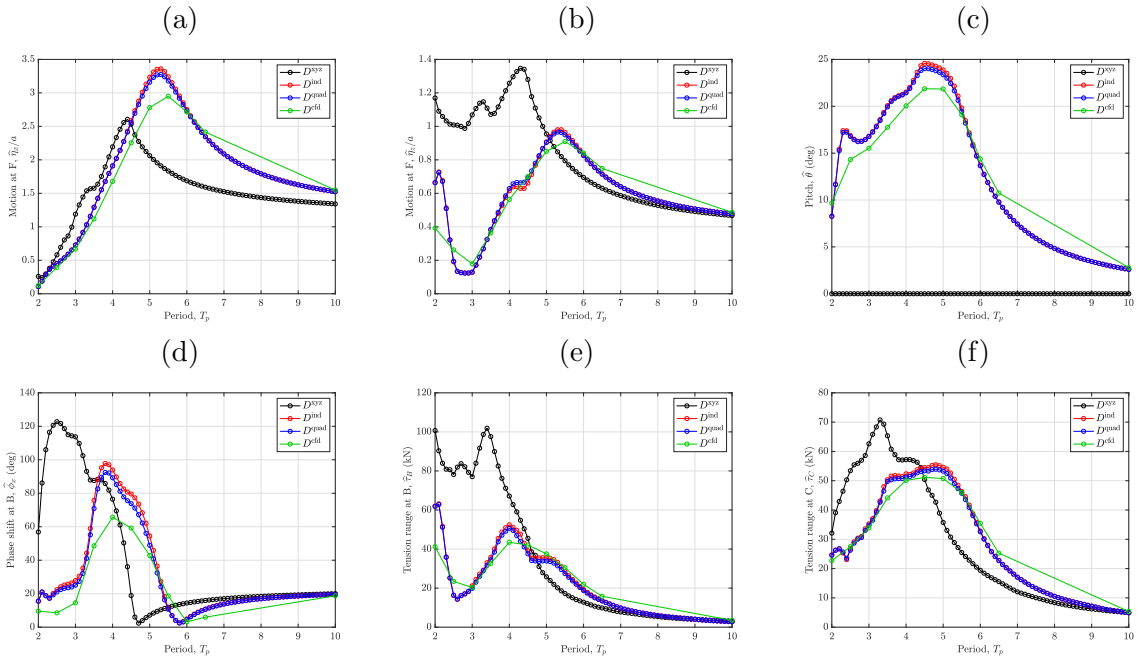

Figure 3: Envelope results for the the cylinder. (a),(b) and (c) show buoy motion amplitudes $\widehat{\eta}_x$, $\widehat{\eta}_z$ and pitch ($\widehat{\theta}$) respectively. (d) shows the phase difference between fairlead motion and motion of point B. (a)-(c) compare the Fourier amplitudes at the driving frequency. (e) and (f) compare the dynamic tension range ($\max(T) - \min(T)$) at point B of cable 1 and at point C of cable 2 respectively.

predicted motion amplitudes of the buoy are overall smaller in the *cfd* model than in the Morison approaches.

To further illustrate the importance of high-fidelity simulations we consider the vorticity around the cylinder. Figure 4 shows that even around a simple geometric form in moderate motion amplitude (fairlead amplitude is $a = 0.5$ m), the vortical influence can clearly be seen. For cases where the mooring system is fitted with large floaters or clump-weight, the importance of mooring component fidelity on the device motion and overall responses is clearly illustrated.

3.2 Catenary chain in current

A comprehensive experimental parameter study of catenary moorings was performed by Barrera *et al.* [14]. They investigated the influence of catenary weight, fairlead motion, currents, waves, bottom friction etc. The chains are submerged in the wave and current flume at IH Cantabria, Spain, and are Froude scaled to a 1:40 scale. The flume is 56 m long (but truncated to 24 m in the CFD model) and has a water depth of 1.35 m. The catenary chain investigated here is 7.305 m long, with a mass of 0.115 kg/m, an equivalent diameter of 0.0033 m and a Young's modulus of $E = 15.6$ GPa. In the experimental set-up a spring is attached to the anchor, but as we do not have details about the rest lengths and pretension we disregard the spring. This will give a more stiff mooring system but the overall characteristics will be captured. The anchor is located at $\mathbf{x}_a = (0, 0, 0)$ m and the fairlead at rest at $\mathbf{x}_f = (6.97, 0, 1.2)$ m. As we are interested

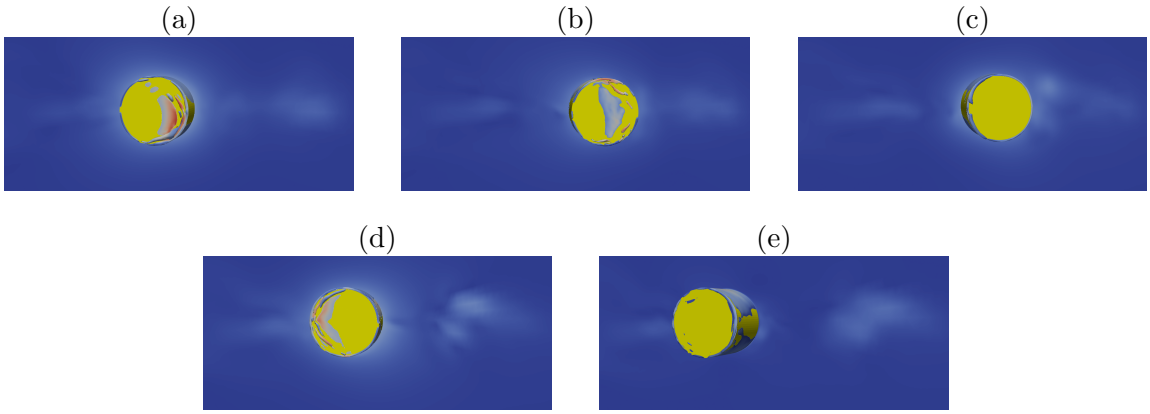

Figure 4: Top view of the CFD simulations of the submerged buoy at z=$h^b/2$ with the Q=200 iso-surface. Colors are by velocity magnitude $U \in [0, 4.3]$ m/s (blue to red). The snap shots were taken 0.2 time periods apart over one cycle: (a) $t/T_p = 0.0$; (b) $t/T_p = 0.2$; (c) $t/T_p = 0.4$; (d) $t/T_p = 0.6$ and (e) $t/T_p = 0.8$;

in the fluid sampling we simulate the case of a steady current of 0.08 m/s. For simplicity we here assume the current to be uniform. At the fairlead a sinusoidal surge motion with amplitude 0.075 m is imposed for a number of different periods $T_f = [0.79, 1.58, 2.37, 3.16, 4.74]$ s.

The chain is divided into $N_{el} = 20$ elements of order $P = 4$ and the mooring simulations are done using a CFL condition of 0.9. The fluid part is modelled as a quasi 2D domain made up of 430 000 rather uniform hexahedrals.

Figure 5 shows the time history of the tension at the fairlead using (i) no current, (ii) a uniform current inside Moody, and (iii) sampling the current from the CFD domain. We see that we get a slight difference in the peak load, the current gives a larger peak load. This effect diminishes with increasing T_f. As expected there are only very minute differences between the CFD sampling and the internal uniform current, which verifies the fluid sampling procedure inside the OpenFOAM solver. The differences arise mainly due to: (i) that the fluid velocity close to the bottom differs ; and (ii) that some nodes exits the CFD domain (very small value below the bottom) and experience zero fluid velocity in the sampled simulation. The numerical noise seen in the low-tension region of Figure 5 is attributed to ground-model interaction issues in the high-order formulation of Moody.

Comparing the numerical simulations to the experimental data from [14], we can see that we have larger max peaks and less difference between current and still water in the simulations (see Figure 6). This is believed to be due to assumptions made in the numerical set up, such as the disregard of the spring at the anchor and the approximation of uniform flow. Nevertheless, the general behavior of the maximum and minimum tension and the effect of current is captured in the numerical model.

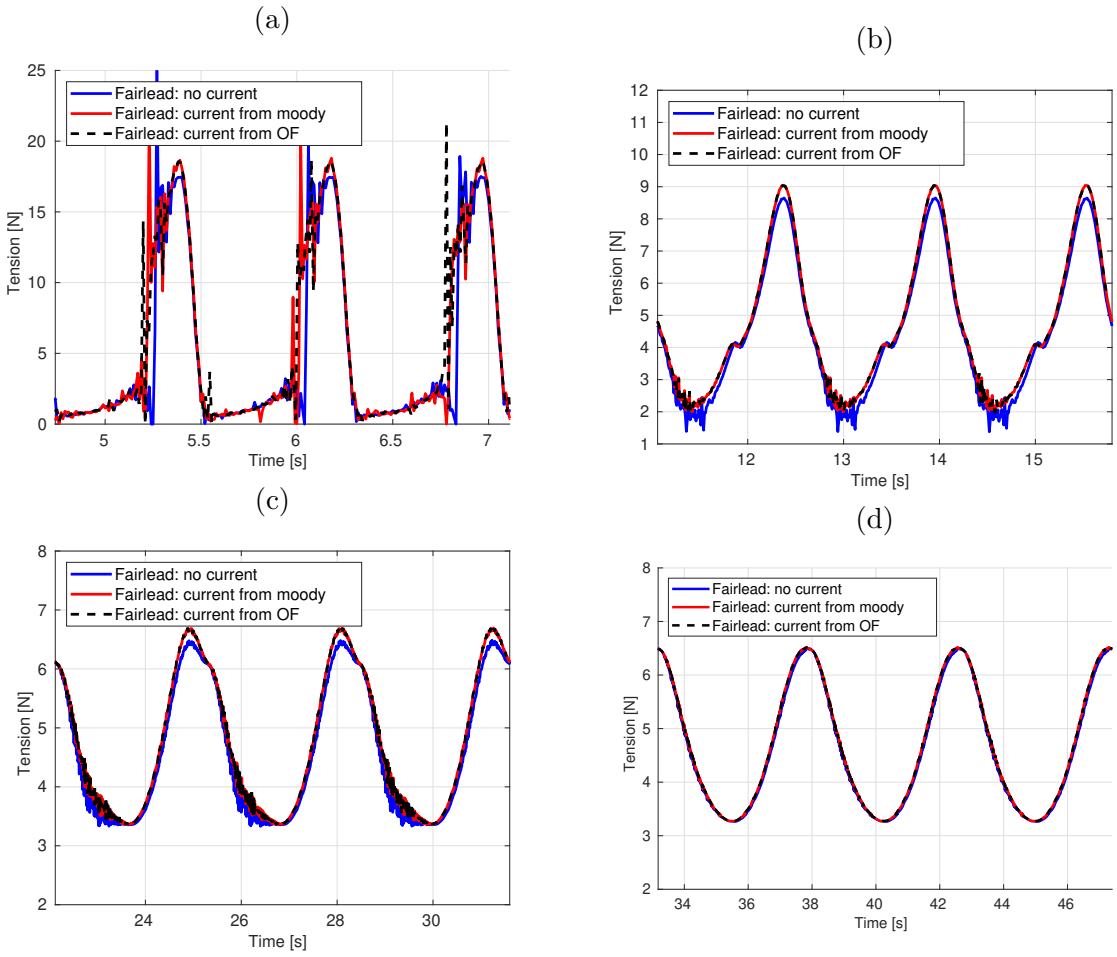

Figure 5: Time history of the tension in the fairlead for the case of no current, uniform current inside the Moody mooring solver and uniform current sampled from the OpenFOAM CFD solver. Sinusoidal surge motion of the fairlead with 0.075 m amplitude and periods of (a) $T_f = 0.79$ s, (b) $T_f = 1.58$ s, (c) $T_f = 3.16$ s and (d) $T_f = 4.74$ s.

3.3 OC5 floating offshore wind turbine

A much studied floating offshore wind turbine (FOWT) case is the DeepCwind semisubmersible that has been used in the OC5-OC6 projects in the International Energy Agency (IEA) Wind Task 30 [15, 9]. DeepCwind is slack moored with three catenaries 120 degrees apart and the front catenary is aligned in the wave direction (see Figure 7). The case is a 1:50 scale model tested at the wave basin at Marin, the Netherlands. The OC5 case has been modelled using the CFD solver ReFRESCO in a series of papers by Burmester *et al.* [7, 16]. Most of the studies has focused on verification and validation (V&V) of the CFD method with the mooring only represented as simple restoring forces, but in the recent study [7] the CFD model ReFRESCO was coupled to the dynamic mooring solver aNySIM to model the OC5 case. Another study focusing on numerical uncertainties is the V&V study [17] using bi-chromatic waves in the STAR-CCM+

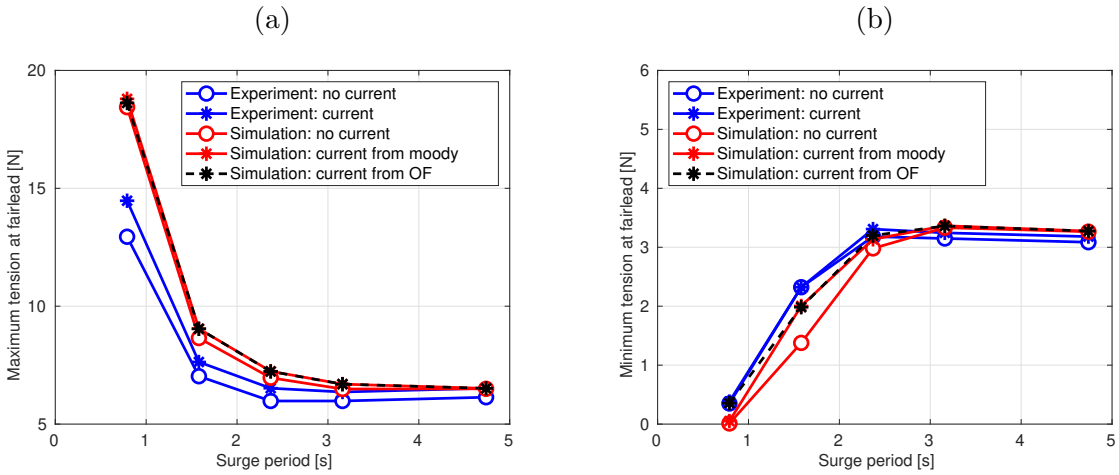

Figure 6: Maximum (a) and minimum (b) fairlead tension for the case of no current, uniform current inside the Moody mooring solver and uniform current sampled from the OpenFOAM CFD solver. Sinusoidal surge motion of the fairlead with 0.075 m amplitude and period T_f s. Experimental data from [14].

model. Very recently Martin and Bihs [8] simulated this case using a mooring model based on finite difference discretization of a geometric exact beam model coupled to the REEF3D CFD model. It is worth to note that this model does sample the fluid dynamics to be used in the mooring drag and inertia.

The FOWT is set-up in OpenFOAM in a hexahedral dominated mesh. The mesh is rather coarse consisting of 2M cells and only two cells in the boundary layer. Thus, the results presented below is of preliminary nature. We generate regular waves with wave height of 0.147 m and period of 1.71 s using the native wave generation in OpenFOAM-v2012. The three catenaries are each discretised into 10 elements of order 4. See Table 1 for information about the data parameters of the semi-submersible and the mooring used in the simulation.

Table 1: Parameters for the OC5 case in model scale.

Semi-submersible		Mooring	
Mass	111.66 kg	Mass	50.2E-03 kg/m
CoG	(0 0 -0.161) m	Eqv. diameter	2.77E-03 m
I_{yy}	49.77 kgm^2	Stiffness	5.98E03 N
		Length	16.71 m

Figure 8 show a time history of the tension at the fairlead for the forward catenary for simulations with and without fluid sampling from the CFD domain. First we note that the tensions are generally similar between the simulations but there are differences. We believe the differences to be exaggerated in these simulations due to a faulty restart of the mooring solver in the model that samples the fluid domain. It is also interesting to compare to the result of [8].

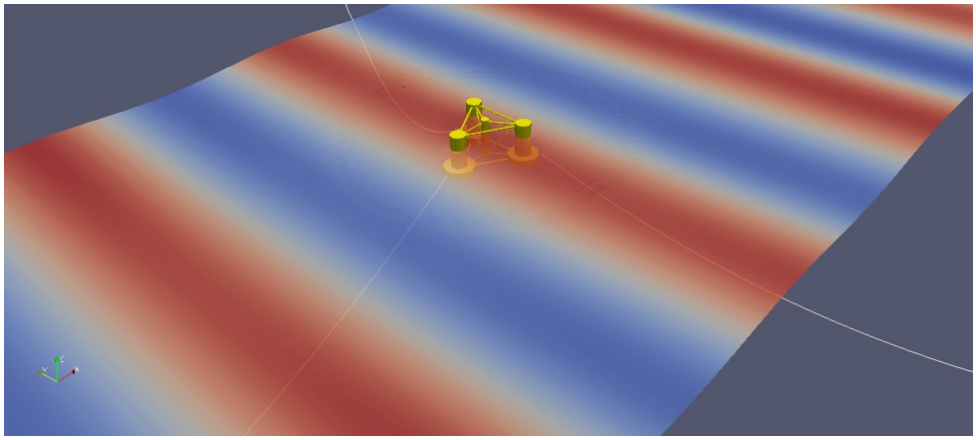

Figure 7: Snapshot of slack-moored OC5 FOWT in regular waves ($H = 0.147$ m and $T = 1.71$. s) propagating in the positive x-direction.

Even though the two studies uses slightly different wave cases the tension response is similar with clear high-order terms. This is in contrast to the reference mooring solutions presented in [8].

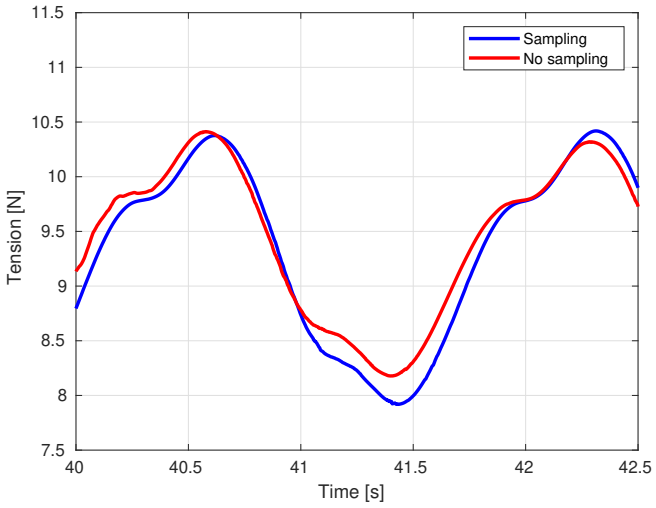

Figure 8: Tension at the fairlead of the front mooring line.

4 CONCLUSIONS

Mooring lines are slender structures and the one-way coupling has a high degree of accuracy for most mooring applications. For cases where the current has a strong spatial variation, the one-way sampling effectively transmits the CFD domain flow resolution to the dynamic mooring

response. The sampling also takes care of the problem of near-field disturbance of the wave-field close to larger structures or complex geometries. In such cases, an analytic approximation based on assuming still water or an undisturbed incoming wave-field are both uncertain, and the one-way implementation guarantees a much more representative flow to estimate the fluid loads on the moorings. Of course, the benefit is highest close to the body and is less important for the lower parts of the mooring lines. For use with e.g. vortex induced motion (VIM) there should, however, be a two-way coupling for the mooring lines. Presently we are working on implementing the Eulerian-Lagrangian approach as presented by Martin *et al.* [18] for two-way coupling of net structures.

Finally, it should be mentioned that even though the sampling has been developed for coupling OpenFOAM with Moody, the sampling functionalities are straightforward to use for any other mooring solver, by just adding a few routines to the mooring solver API (to send the mooring nodes to the CFD solver and to set the sampled fluid velocities in the mooring). These updates are included in the next release of Moody (v2.1). Moody and the OpenFOAM sampling routines will be available through github (`https://github.com/johannep/moodyAPI`) and from the CCP-WSI repository (`https://www.ccp-wsi.ac.uk`).

REFERENCES

[1] Orcina Ltd. *OrcaFlex Manual-Version 9.7a* (2015).

[2] ANSYS Inc. *AQWA theory manual 19.1* (2018).

[3] Yu, Y. and Li, Y. Preliminary results of a RANS simulation for a floating point absorber wave energy system under extreme wave conditions. In: *Proc. OMAE 2011* (2011).

[4] Ransley, E., Yan, S., Brown, S., Hann, M., Graham, D., Windt, C., Schmitt, P., Davidson, J., Ringwood, J., Musiedlak, P.-H. Wang, J., Wang, J., Ma, Q., Xie, Z., Zhang, N., Zheng, X., Giorgi, G., Chen, H., Lin, X., Qian, L., Ma, Z., Bai, W., Chen, Q., Zang, J., Ding, H., Cheng, L., Zheng, J., Gu, H., Gong, X., Liu, Z., Zhuang, Y., Wan, D., Bingham, H. and Greaves, D. A blind comparative study of focused wave interactions with floating structures (CCP-WSI Blind Test Series 3). *International Journal of Offshore and Polar Engineering* (2020) **30**(1):1–10.

[5] Palm, J., Eskilsson, C., Paredes, G.M. and Bergdahl, L. CFD simulation of a moored floating wave energy converter. In: *Proceedings of the 10th European Wave and Tidal Energy Conference* (2013).

[6] Palm, J., Eskilsson, C., Paredes G.M. and Bergdahl, L. Coupled mooring analysis of floating wave energy converters using CFD: Formulation and validation. *Int. J. Marine Energy* (2016) **16**:83–99.

[7] Burmester, S., Vaz, G., el Moctar, O., Gueydon, S., Koop,A., Wang, Y. and Chen, H.C. High-fidelity modelling of floating offshore wind turbine platforms. In: *Proceedings of the 39th International Conference on Ocean, Offshore & Arctic Engineering* (2020).

[8] Martin, T. and Bihs, H. A numerical solution for modelling mooring dynamics, including bending and shearing effects, using a geometrically exact beam model. *J. Mar. Sci. Eng.* (2021) **9**:486.

[9] Robertson, A., Bachynski, E.E., Gueydon, S., Wendt, F. and Schünemann, P. Total experimental uncertainty in hydrodynamic testing of a semisubmersible wind turbine, considering numerical propagation of systematic uncertainty. *Ocean Engineering* (2020) **195**:106605.

[10] Palm, J. and Eskilsson, C. *Moody, User's Manual – v2.1*, Sigma Energy & Marine and RISE, Sweden, (2021).

[11] Morison, J.R., O'Brien, M.P., Johnson, J.W. and Schaaf, S.A. The force exerted by surface waves on piles. *Petroleum Transactions, Amer. Inst. Mining Engineers* (1950) **186**:149–154.

[12] Palm, J., Eskilsson, C. and Bergdahl, L. An *hp*-adaptive discontinuous Galerkin method for modelling snap loads in mooring cables. *Ocean Engng.* (2017) **144**:266–276.

[13] Palm, J. and Eskilsson, C. Mooring systems with submerged buoys: influence of floater geometry and model fidelity. *App. Ocean Res.* (2020) **102**:102302.

[14] Barrera, C., Guanche, R. and Losada, I.J. Experimental modelling of mooring systems for marine energy concepts. *Marine Structures* (2019) **63**:153–180.

[15] Robertson, A., Wendt, F., Jonkman, J., Popko, W., Dagher, H., Gueydon, S., Qvist, J., Vittori, F., Uzunogulo, E. and Harries, R. OC5 project phase II: Validation of global loads of the DeepCwind floating semisubmersible wind turbine. *Energy Procedia* (2017) **137**:38–57.

[16] Wang, Y., Chen, H.C., Vaz, G. and Burmester, S. CFD simulation of semi-submersible floating offshore wind turbine under regular waves. In:*Proceedings of ISOPE* (2020).

[17] Wang, L., Robertson, A., Jonkman, J. and Yu, Y. Uncertainty assessment of CFD investigation of the nonlinear difference-frequency wave loads on a semisubmersible FOWT platform. *Sustainability* (2021) **13**:64.

[18] Martin, T., Kamath, A. and Bihs, H. A Lagrangian approach for the coupled simulation of fixed net structures in a Eulerian fluid model. *Journal of Fluids and Structures* (2020) **94**:102962.